REPORT DOCUMENTATION PAGE

Form Approved OMB NO. 0704-0188

1. REPORT DATE (DD-MM-YYYY)	2. REPORT TYPE	3. DATES COVERED (From - To)
05-10-2018	Final Report	1-Sep-2016 - 31-Aug-2018

4. TITLE AND SUBTITLE
Final Report: Fundamental Studies of Single Photon Detection with Avalanche Photodiodes

5a. CONTRACT NUMBER
W911NF-16-2-0178

5b. GRANT NUMBER

5c. PROGRAM ELEMENT NUMBER

6. AUTHORS

5d. PROJECT NUMBER

5e. TASK NUMBER

5f. WORK UNIT NUMBER

7. PERFORMING ORGANIZATION NAMES AND ADDRESSES
University of Virginia
1001 North Emmet Street
P. O. Box 400195
Charlottesville, VA 22904 -4195

8. PERFORMING ORGANIZATION REPORT NUMBER

9. SPONSORING/MONITORING AGENCY NAME(S) AND ADDRESS (ES)
U.S. Army Research Office
P.O. Box 12211
Research Triangle Park, NC 27709-2211

10. SPONSOR/MONITOR'S ACRONYM(S)
ARO

11. SPONSOR/MONITOR'S REPORT NUMBER(S)
69710-PH-DRP.1

12. DISTRIBUTION AVAILIBILITY STATEMENT
Approved for public release; distribution is unlimited.

13. SUPPLEMENTARY NOTES
The views, opinions and/or findings contained in this report are those of the author(s) and should not contrued as an official Department of the Army position, policy or decision, unless so designated by other documentation.

14. ABSTRACT

15. SUBJECT TERMS

16. SECURITY CLASSIFICATION OF:			17. LIMITATION OF ABSTRACT	15. NUMBER OF PAGES	19a. NAME OF RESPONSIBLE PERSON
a. REPORT	b. ABSTRACT	c. THIS PAGE			Joe Campbell
UU	UU	UU	UU		19b. TELEPHONE NUMBER 434-243-2068

RPPR Final Report
as of 28-Oct-2018

Agency Code:

Proposal Number: 69710PHDRP **Agreement Number: W911NF-16-2-0178**
INVESTIGATOR(S):

Name: Joe Campbell
Email: jcc7s@virginia.edu
Phone Number: 4342432068
Principal: Y

Organization: **University of Virginia**
Address: 1001 North Emmet Street, Charlottesville, VA 229044195
Country: USA
DUNS Number: 065391526 EIN: 546001796

Report Date: 30-Nov-2018 Date Received: 05-Oct-2018
Final Report for Period Beginning 01-Sep-2016 and Ending 31-Aug-2018
Title: Fundamental Studies of Single Photon Detection with Avalanche Photodiodes
Begin Performance Period: 01-Sep-2016 **End Performance Period:** 31-Aug-2018
Report Term: 0-Other

Submitted By: Joe Campbell Email: jcc7s@virginia.edu
Phone: (434) 243-2068

Distribution Statement: 1-Approved for public release; distribution is unlimited.

STEM Degrees: **STEM Participants:**

Major Goals: The goal of this program was to conduct fundamental studies of single photon detection with avalanche photodiodes.

Accomplishments: Theory effort:
Pfister's group carried out the theoretical evaluation of the photon-count positive-operator-valued measurements for the segmented detector. Results showed that photon number resolution detection is indeed achievable in the ideal case. This opens a new path to photon number resolution devices that operate at room temperature and can be manufactured with available integrated photonic technology. The number of integrated APDs appears to be, to a large extent, the dominant factor toward high-quality photon number resolution detection. While photon losses must also be taken in to account, of course, it is important to note that they do not include the quantum efficiency of the APDs, by design of the segmented detector. The reduction of photon losses will therefore only involve passive optical design considerations, a notable difference with butt-coupled tree-splitting detectors. Details of this work are provided in Appendix 1: "Photon-number-resolving segmented avalanche-photodiode detectors."

Segmented avalanche photodiodes:
A novel segmented waveguide photodetector based on a directional coupler design was developed and demonstrated. By matching the imaginary parts of the propagation constants of the even and odd modes in the design, a 6-element photodiode array achieved an internal responsivity as high as 1.13 A/W in agreement with simulations. This design can be extended to applications in travelling wave photodiodes and in the photon number resolving detectors that were studied in this program owing to their near-unity quantum efficiency and minimized active volumes. Details of this work are provided in Appendix 2: "Segmented waveguide photodetector with 90% quantum efficiency."

Training Opportunities: Nothing to Report

Results Dissemination: Nothing to Report

Honors and Awards: Nothing to Report

Protocol Activity Status:

Technology Transfer: Nothing to Report

RPPR Final Report
as of 28-Oct-2018

PARTICIPANTS:

Participant Type: Co PD/PI
Participant: Olivier Pfister
Person Months Worked: 2.00 **Funding Support:**
Project Contribution:
International Collaboration:
International Travel:
National Academy Member: N
Other Collaborators:

Participant Type: Co PD/PI
Participant: Andreas Beling
Person Months Worked: 2.00 **Funding Support:**
Project Contribution:
International Collaboration:
International Travel:
National Academy Member: N
Other Collaborators:

Participant Type: Co PD/PI
Participant: Seth Bank
Person Months Worked: 2.00 **Funding Support:**
Project Contribution:
International Collaboration:
International Travel:
National Academy Member: N
Other Collaborators:

Participant Type: PD/PI
Participant: Joe Campbell
Person Months Worked: 2.00 **Funding Support:**
Project Contribution:
International Collaboration:
International Travel:
National Academy Member: Y
Other Collaborators:

REPORT DOCUMENTATION PAGE (Standard Form 298)

REPORT DOCUMENTATION PAGE	Form Approved OMB No. 0704-0188

The public reporting burden for this collection of information is estimated to average 1 hour per response, including the time for reviewing instructions, searching existing data sources, gathering and maintaining the data needed, and completing and reviewing the collection of information. Send comments regarding this burden estimate or any other aspect of this collection of information, including suggestions for reducing the burden, to Department of Defense, Washington Headquarters Services, Directorate for Information Operations and Reports (0704-0188), 1215 Jefferson Davis Highway, Suite 1204, Arlington, VA 22202-4302. Respondents should be aware that notwithstanding any other provision of law, no person shall be subject to any penalty for failing to comply with a collection of information if it does not display a currently valid OMB control number.
PLEASE DO NOT RETURN YOUR FORM TO THE ABOVE ADDRESS.

1. REPORT DATE *(DD-MM-YYYY)*	2. REPORT TYPE	3. DATES COVERED *(From - To)*
10/5/18	Final report	9/1/16-8/31/18

4. TITLE AND SUBTITLE	5a. CONTRACT NUMBER
Fundamental Studies of Single Photon Detection with Avalanche Photodiodes	W911NF-16-2-0178
	5b. GRANT NUMBER
	5c. PROGRAM ELEMENT NUMBER
6. AUTHOR(S)	5d. PROJECT NUMBER
Joe C. Campbell	5e. TASK NUMBER
	5f. WORK UNIT NUMBER

7. PERFORMING ORGANIZATION NAME(S) AND ADDRESS(ES)	8. PERFORMING ORGANIZATION REPORT NUMBER
University of Virginia Department of Electrical and Computer Engineering Charlottesville, VA 22904	
9. SPONSORING/MONITORING AGENCY NAME(S) AND ADDRESS(ES)	10. SPONSOR/MONITOR'S ACRONYM(S)
DARPA/ARO	11. SPONSOR/MONITOR'S REPORT NUMBER(S)

12. DISTRIBUTION/AVAILABILITY STATEMENT
No restrictions

13. SUPPLEMENTARY NOTES

14. ABSTRACT
The goal of this program was to conduct fundamental studies of single photon detection with avalanche photodiodes.

15. SUBJECT TERMS

16. SECURITY CLASSIFICATION OF:			17. LIMITATION OF ABSTRACT	18. NUMBER OF PAGES	19a. NAME OF RESPONSIBLE PERSON
a. REPORT	b. ABSTRACT	c. THIS PAGE			19b. TELEPHONE NUMBER *(Include area code)*

Standard Form 298 (Rev. 8/98)
Prescribed by ANSI Std. Z39.18

INSTRUCTIONS FOR COMPLETING SF 298

1. REPORT DATE. Full publication date, including day, month, if available. Must cite at least the year and be Year 2000 compliant, e.g. 30-06-1998; xx-06-1998; xx-xx-1998.

2. REPORT TYPE. State the type of report, such as final, technical, interim, memorandum, master's thesis, progress, quarterly, research, special, group study, etc.

3. DATE COVERED. Indicate the time during which the work was performed and the report was written, e.g., Jun 1997 - Jun 1998; 1-10 Jun 1996; May - Nov 1998; Nov 1998.

4. TITLE. Enter title and subtitle with volume number and part number, if applicable. On classified documents, enter the title classification in parentheses.

5a. CONTRACT NUMBER. Enter all contract numbers as they appear in the report, e.g. F33315-86-C-5169.

5b. GRANT NUMBER. Enter all grant numbers as they appear in the report. e.g. AFOSR-82-1234.

5c. PROGRAM ELEMENT NUMBER. Enter all program element numbers as they appear in the report, e.g. 61101A.

5e. TASK NUMBER. Enter all task numbers as they appear in the report, e.g. 05; RF0330201; T4112.

5f. WORK UNIT NUMBER. Enter all work unit numbers as they appear in the report, e.g. 001; AFAPL30480105.

6. AUTHOR(S). Enter name(s) of person(s) responsible for writing the report, performing the research, or credited with the content of the report. The form of entry is the last name, first name, middle initial, and additional qualifiers separated by commas, e.g. Smith, Richard, J, Jr.

7. PERFORMING ORGANIZATION NAME(S) AND ADDRESS(ES). Self-explanatory.

8. PERFORMING ORGANIZATION REPORT NUMBER. Enter all unique alphanumeric report numbers assigned by the performing organization, e.g. BRL-1234; AFWL-TR-85-4017-Vol-21-PT-2.

9. SPONSORING/MONITORING AGENCY NAME(S) AND ADDRESS(ES). Enter the name and address of the organization(s) financially responsible for and monitoring the work.

10. SPONSOR/MONITOR'S ACRONYM(S). Enter, if available, e.g. BRL, ARDEC, NADC.

11. SPONSOR/MONITOR'S REPORT NUMBER(S). Enter report number as assigned by the sponsoring/ monitoring agency, if available, e.g. BRL-TR-829; -215.

12. DISTRIBUTION/AVAILABILITY STATEMENT. Use agency-mandated availability statements to indicate the public availability or distribution limitations of the report. If additional limitations/ restrictions or special markings are indicated, follow agency authorization procedures, e.g. RD/FRD, PROPIN, ITAR, etc. Include copyright information.

13. SUPPLEMENTARY NOTES. Enter information not included elsewhere such as: prepared in cooperation with; translation of; report supersedes; old edition number, etc.

14. ABSTRACT. A brief (approximately 200 words) factual summary of the most significant information.

15. SUBJECT TERMS. Key words or phrases identifying major concepts in the report.

16. SECURITY CLASSIFICATION. Enter security classification in accordance with security classification regulations, e.g. U, C, S, etc. If this form contains classified information, stamp classification level on the top and bottom of this page.

17. LIMITATION OF ABSTRACT. This block must be completed to assign a distribution limitation to the abstract. Enter UU (Unclassified Unlimited) or SAR (Same as Report). An entry in this block is necessary if the abstract is to be limited.

Fundamental Studies of Single Photon Detection with Avalanche Photodiodes

W911NF1620178

Final Report

Department of Electrical and Computer Engineering
The University of Virginia
Charlottesville, VA 22904-4743

Technical Point of Contact:
Joe C. Campbell
Dept. Electrical and Computer Engineering
University of Virginia
Thornton Hall, E219
Charlottesville, VA 22904
Telephone: (434)-243-2068
jcc7s@virginia.edu

Administrative Point of Contact:
Rob Merhige
Director of Grants & Contracts
University of Virginia
PO Box 400195
Carruthers Hall
Charlottesville, VA 22903
Telephone: (434) 924-6142
rrm9u@virginia.edu

Key personnel:

Joe Campbell	University of Virginia
Andreas Beling	University of Virginia, Department of Electrical and Computer Engineering, Charlottesville, VA 22904, ab3pj@eservices.virginia.edu
Olivier Pfister	University of Virginia, Department of Physics, Charlottesville, VA 22904, opfister@virginia.edu
Seth Bank	University of Texas at Austin, Department of Electrical and Computer Engineering, 1 University Station C0803, Austin, TX 78712, sbank@ece.utexas.edu

Contractor Type: University of Virginia – other educational
Subcontractor types: University of Texas at Austin – other educational

Table of Contents

List of Appendixes

Statement of the Problem

The goal of this program was to conduct fundamental studies of single photon detection with avalanche photodiodes. The primary thrust was to develop a fundamental theory of single photon detection with emphasis on temporal precision, maximum rate, bandwidth, detection efficiency, and photon-number resolution. Olivier Pfister's group at the University of Virginia lead this effort. The specific thrust of his study was the realistic implementation of a quantum mechanical model for photon-number-resolved detection with non-ideal non-photon-number-resolving detectors. For monochromatic light, the modes are defined by the wavevector, frequency, and polarization. The probability amplitude density for detecting photons in a given wave, i.e. the "photon wavefunction", is then given by the precise mode function of its electric field.[1] In classical optics both spatial and temporal mode matching are crucially important for quantum optics: indeed, in order to achieve 100% photon detection efficiency, one must take into account two types of quantum probabilities: first, *the energy transfer overlap* in the detector material itself. This is often the only overlap considered to determine the quantum efficiency of photodetection, in which the photon is annihilated and its energy transferred to the detector material (here by creating an electron-hole pair in a semiconductor), but this is not enough. One must also take into account *the mode-matching overlap* between the source field mode and the detector response function, as it yields the probability of finding one (or several) photon(s) in a given region of space, during a given time interval (where and when the detector is, respectively, present and active). This also affects the detection bandwidth. Another fundamental concept, which affects maximum detection rate and photon-number resolution (PNR), is the splitting of the field between several independent detectors.

The Pfister group also investigated quantum-engineering field splitting by designing unitary transformations more general than beam splitters and exploring beam splitters seeded with quantum light. This approach involved developing a general unitary transformation, which is formulated as the following general *quantum engineering* problem: given N detector modes, is there a way to design a unitary transformation of the quantum field that takes the N-mode input state $|n\rangle_1|0\rangle_2\ldots|0\rangle_N$ (assuming $n<N$) to the ideal output $|1\rangle_1|1\rangle_2\ldots|1\rangle_n|0\rangle_{n+1}\ldots|0\rangle_N$? The next

question is whether superpositions of such inputs can be accommodated as well. This is not a trivial question but solving it would be a major enabler of photon-number-resolving detection by ensuring that no more than one photon ever enters any of the split photodetection channels. The importance of this approach is its universality, being independent of the detector type.

Linear-mode operation refers to APDs biased below breakdown. In linear-mode the response is analog. APDs biased above breakdown function as optically triggered digital switches; this is referred to as Geiger-mode and the devices are designated as single photon avalanche diodes (SPADs). Operation in the linear mode requires the APD to be followed by a pre-amplifier. In order to achieve a signal 10 dB above the noise floor of the lowest noise pre-amplifiers available, it is necessary to inject electrical pulses of approximately 1000 electrons in a 1 ns pulse, i.e., the APD needs to operate at a gain, M, of at least 1000. It is well known that the mean-squared shot-noise current can be expressed as[2] $\langle i_{shot}^2 \rangle = 2q(I_{ph}+I_{dark})M^2F(M)\Delta f$ where I_{ph} and I_{dark} are the primary photocurrent and dark current, respectively, Δf is the bandwidth, and F(M) is the excess noise factor. In the local field model[2] the excess noise factor is given by $F(M) = kM+(1-k)[2-1/M]$, where k is the ratio of the electron, α, and hole, β, ionization coefficients such that by convention $k = \beta/\alpha$ if $\beta < \alpha$ and α/β if $\beta > \alpha$. For the case of M = 1000, the 10 dB signal to noise ratio imposes a restriction of $k \leq 0.015$ on the material from which the APD is fabricated. Both InAs[3,4] and $Hg_{0.7}Cd_{0.3}Te$ [5] have exhibited k values this low, however, even in the absence of generation-recombination centers, the diffusion current prevents anything close to 1 dark count per second even at 77K. Therefore, the high dark current for these low-k-value materials is essentially intrinsic to their band structure and there is little chance of achieving the requisite gain levels with low dark counts. Current InAs and $Hg_{0.7}Cd_{0.3}Te$ structures are also incompatible with the jitter and detection rate goals of this program. In summary, there are fundamental materials limitations that prevent linear-mode APDs from achieving the performance metrics specified for this program.

The preponderance of semiconductor-based single-photon detectors reported to date is SPADs. The most advanced and highest performing materials for SPADs are Si, for detection between 300 nm and 950 nm, and InGaAs, for detection between 925 nm and 1650 nm. A handful of other materials are suitable for UV operation, notably SiC, and for mid-IR single-photon detection HgCdTe has been used. SPADs can be operated usefully with low-power thermoelectric cooling, and individual state-of-the-art demonstrations have achieved efficiencies up to 85 % at 670 nm, timing resolution of 18 ps, dark count rates of 1 s^{-1}, photon count rates above 10^8 s^{-1} in a gated mode and above 10^6 s^{-1} free-running, and large arrays (> 10^3 elements). None of these performance metrics have been achieved simultaneously in a single SPAD. Properties of SPADs are often interrelated, and performance tradeoffs are commonly made.

For SPADs the most challenging program metrics were the 1 cps dark count rate and 100 fs jitter. It is clear that in order to achieve these metrics, it is necessary to reduce the active volume

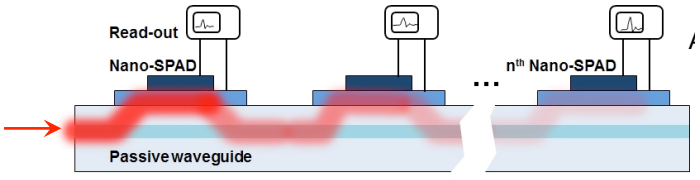

Figure 1. Schematic of a segmented nano-waveguide SPAD.

while maintaining ~ 100% detection efficiency. Guided by the quantum model developed by Pfister's group, we pursued the following strategy: using several nano-detectors in series, i.e., a segmented detector (Fig. 1(a)). The segmented detector employs a novel adiabatic optical coupling scheme that is based on a nanometer-scale inverse tapered waveguide underneath the detector. Simulations show that ~ 100% coupling efficiencies can be achieved. As a result, this approach has the potential to reach near-unity quantum efficiency with ~ 1 μm^3 detector volumes. Photons that are not absorbed in the first SPAD couple back into the waveguide and will be absorbed in one of the following SPADs. Since the array is essentially a long detector divided into *N* short detectors, each with an individual read-out, the dark count rate and jitter can be as low as 1 cps and <1 ps, respectively.

Summary of Important Results

Theory effort:
Pfister's group carried out the theoretical evaluation of the photon-count positive-operator-valued measurements for the segmented detector. Results showed that photon number resolution detection is indeed achievable in the ideal case. This opens a new path to photon number resolution devices that operate at room temperature and can be manufactured with available integrated photonic technology. The number of integrated APDs appears to be, to a large extent, the dominant factor toward high-quality photon number resolution detection. While photon losses must also be taken in to account, of course, it is important to note that they do not include the quantum efficiency of the APDs, by design of the segmented detector. The reduction of photon losses will therefore only involve passive optical design considerations, a notable difference with butt-coupled tree-splitting detectors. Details of this work are provided in Appendix 1: "Photon-number-resolving segmented avalanche-photodiode detectors."

Segmented avalanche photodiodes:
A novel segmented waveguide photodetector based on a directional coupler design was developed and demonstrated. By matching the imaginary parts of the propagation constants of the even and odd modes in the design, a 6-element photodiode array achieved an internal responsivity as high as 1.13 A/W in agreement with simulations. This design can be extended to applications in travelling wave photodiodes and in the photon number resolving detectors that were studied in this program owing to their near-unity quantum efficiency and minimized active volumes. Details of this work are provided in Appendix 2: "Segmented waveguide photodetector with 90% quantum efficiency."

Bibliography

[1] M. Scully and A. Zubairy, Quantum Optics, Cambridge University Press (1997).
[2] McIntyre, R. J., IEEE Trans. Electron Dev. **ED-13**, 64 (1966).

[3] Wenlu Sun, Scott J. Maddox, Seth R. Bank, and Joe C. Campbell, 72nd Device Research Conference, 47, Santa Barbara, CA. (2014).
[4] A. R. J. Marshall, et al., Optics Express **19**, 23341 (2011).
[5] J. D. Beck, et al., Proc. 2003 IEEE LEOS Annual Mtg. **2**, 849 (2003).

Appendix 1. Photon-number-resolving segmented avalanche-photodiode detectors

Photon-number-resolving segmented avalanche-photodiode detectors

Rajveer Nehra,[1] Chun-Hung Chang,[1] Andreas Beling,[2] and Olivier Pfister[1]

[1] *Department of Physics, University of Virginia, 382 McCormick Rd, Charlottesville, VA 22903*
[2] *Department of Electrical and Computer Engineering, University of Virginia, 351 McCormick Rd, Charlottesville, VA 22903*

(Dated: August 29, 2017)

We investigate the feasibility and performance of photon-number-resolved photodetection employing avalanche photodiodes (APDs) with low dark counts. The main idea is to split **n** photons over **m** modes such that every mode has no more than one photon, which is detected *alongside propagation* by an APD. We characterize performance by evaluating the purities of positive-operator-valued measurements (POVMs), in terms of APD number and photon loss.

INTRODUCTION

Quantum measurements are essential to quantum technology. Photon-Number-Resolution (PNR) has become a need in various fields including linear optical quantum computing [1], quantum metrology and sensing[2], quantum cryptography [3], quantum imaging[4], and quantum communication [5] and conditional state preparation [6]. A PNR detector produces a signal proportional to the number of incident photons. Currently, PNR detectors can be realized with silicon photomultipliers [7], superconducting nanowires [8–10], linear mode avalanche photodiodes (APDs), quantum-dot field-effect transistors [11, 12], and transtion-edge sensors (TES) [13, 14]. Several methods based on spatial- and time-multiplexing have been proposed for PNR measurements using APDs [10, 15–17].

In this paper we propose a way for PNR using segmented APDs with low dark currents. In the figure shown below we have APDs on waveguide. The set up whittles down n photons, one at a time. Our segmented photodetector

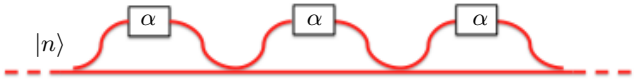

FIG. 1: Segmented detector. Guided optics are used to detect photons alongside propagation by APDs. The design goal is to keep all undetected photons in the waveguide, for further detection.

features multiple APDs fed by the same waveguide, as shown in Fig. 1. Photons that are not absorbed in the first APD couple back into the waveguide and will be absorbed in one of the following detectors. The crucial advantage of this configuration is that nonideal quantum efficiency of the APDs doesn't amount to photon loss, unlike butt-coupled PNR detectors in which temporally or spatially split photons impinge on APDs on the end of their path [15–17]. Hence, this linear array is essentially a long detector divided into m short detectors, each with an individual read-out. We envision that such a segmented photodetector will become feasible in large-scale integrated photonic platforms using either monolithic or heterogeneous integration of APDs on low-loss waveguides.

We will model the segmented detector using beam splitters as shown in Fig.2 where waveguide coupling with APDs can be modeled by the reflectivitys of the beam splitters, and the transmissivity per APD by η. Before we address the model in earnest, we need to re-

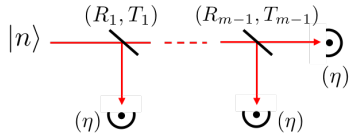

FIG. 2: Model of a PNR segmented photodetector. $R_j + T_j = r_j^2 + t_j^2 = 1, \forall j \in [1, m]$.

iterate that η won't include quantum efficiency of the APD. This can be seen by a detail model of each APD coupling, pictured in Fig.3. The APD's field transmissivity is α (such that the APD's quantum efficiency is $1-\alpha^2$). In fact, α cannot be too large because APDs are not PNR detectors and we want the quantum efficiency $1-\alpha^2 \ll 1/n$, for n incident photons, which will ensure that photons are detected no more than one at a time. In a design reminiscent of interaction-free measurements

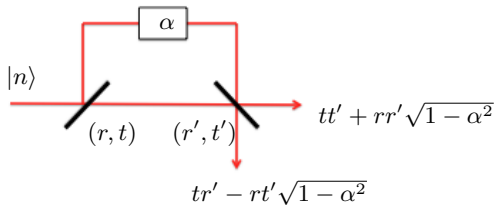

FIG. 3: Model for detection alongside propagation. If this is the j$^{\text{th}}$ APD, then $t_j = tt' + rr'\sqrt{1-\alpha^2}$, where $t_j = T_j^{1/2}$ in Fig.2.

proposed by Elitzur and Vaidman [18], we require that

the bottom output of the exit beam splitter by nulled by destructive interference. The condition can be achieved by choosing parameters (r, t, r', t') of the beam splitters, and absorption coefficient α, such that

$$tr' - rt'\sqrt{1-\alpha^2} = 0. \tag{1}$$

If this is the case, then the detection process truly takes place alongside propagation and finite quantum efficiency — necessary here to attain PNR performance — won't contribute to photon loss.

In the next section, we recall basic properties of the quantum formalism needed to evaluate PNR performance. We then return to the segmented detector model, present our theoretical characterization results, and conclude.

DETECTOR CHARACTERIZATION USING POSITIVE-OPERATOR-VALUED-MEASUREMENTS (POVMS)

The most general measurements in quantum physics are known as POVMs [19, 20]. Each measurement outcome k is given by an Hermitian operator, POVM element $\hat{\Pi}_k$, with nonnegative eigenvalues such that the probability of an outcome for a quantum state $\hat{\rho}$ is given by

$$p_k = Tr(\rho\hat{\Pi}_k). \tag{2}$$

These operators statisfy the completeness property, $\sum_k \hat{\Pi}_k = I$ which makes the sum of probabilities $\sum_k p_k = 1$ for different outcomes to be unity. Therefore, these measurements completely describe all possible outcomes for any quantum measurement. For a phase insensitive detector the POVM element for k clicks is given as

$$\Pi_k = \sum_{n=0} P(k|n)|n\rangle\langle n|, \tag{3}$$

where $P(k|n)$ represents the conditional probability of getting k clicks given n-photon input state. The POVMs are more general from the projective measurements in couple of ways. First, unlike the projective measurements the POVMs are not orthogonal measurements. For outcomes k and k', the pairwise POVMs need not satisfy,

$$\hat{\Pi}_k\hat{\Pi}'_k \neq \delta_{kk'}\Pi_k. \tag{4}$$

Note that the orthogonal POVMs are essentially the projective measurements, therefore we can define the purity of the POVM for outcome k as

$$Purity(\Pi_k) = \frac{\left[Tr(\Pi_k^2)\right]}{\left[Tr(\Pi_k)\right]^2} \tag{5}$$

The purity satisfies $0 \leq Purity(\Pi_k) \leq 1$, where a value of 1 denotes a pure, i.e., projective POVM.

MODEL

In order to study the PNR performance of the segmented detector we consider 2 cases: first, the beam splitters all have the same reflectivity and, second, the reflectivity of the j$^{\text{th}}$ beam splitter is given by $R_j = \frac{1}{m-j+1}$ such that the last beam splitter in Fig.2 in balanced. It can be shown that the field splitting generated by this is identical to that of a symmetric beam splitter tree. We study each case in turn in the lossless case before investigating the symmetric case in the presence of losses.

SEGMENTED DETECTOR WITH IDENTICAL BEAM SPLITTERS

In Fig.2 the quantum input mode has annihilation operator a_1 and is in the input Fock state $|n\rangle$, and the other $m-1$ input modes, of a_2, a_3, ..., a_m, are vacuum ones. We consider $m-1$ identical beam splitters (T, R) and $\eta = 1$ (no losses) for all modes. The input quantum state is

$$|n\rangle = \frac{{a_1^\dagger}^n}{\sqrt{n!}}|0\rangle^{\otimes^m}. \tag{6}$$

In the Heisenberg picture, after m-1 beam splitters $a_1^\dagger$ evolves to

$$\begin{aligned}\underbrace{(U_{m-1}...U_2U_1}_{U}a_1^\dagger\underbrace{U_1^\dagger U_2^\dagger...U_{m-1}^\dagger)}_{U\dagger} \\ = (t^{m-1}a_1^\dagger + rt^{m-2}a_2^\dagger + \cdots + ra_m^\dagger).\end{aligned} \tag{7}$$

It is easy to see that the output quantum state is

$$|\psi\rangle_{out} = \frac{1}{\sqrt{n!}}(Ua_1^\dagger U^\dagger)^n|0\rangle^{\otimes^m} \tag{8}$$

$$= \frac{1}{\sqrt{n!}}(t^{m-1}a_1^\dagger + rt^{m-2}a_2^\dagger + \cdots + ra_m^\dagger)^n|0\rangle^{\otimes^m}. \tag{9}$$

Using multinomial expansion we get

$$|\psi\rangle_{out} = \underbrace{\sum_{n_1=0}^{n}\cdots\sum_{n_m=0}^{n}}_{\sum_{j=1}^m n_j = n}\left\{\frac{\sqrt{n!}}{n_1!n_2!...n_m!}\right. \left.[t^{\sum_{j=1}^m 2(m-j)n_{m-j+1}}r^{(n-n_m)}]\prod_{i=1}^{m}(a_i^\dagger)^{n_i}\right\}|0\rangle^{\otimes^m}, \tag{10}$$

where each n_i can take any value from 0 to n. In order to have PNR each n_i must have at most one photon. The probability of splitting n photons over m modes is

$$P(\{0,1\}^m, n, K) = n!t^{\sum_{j=1}^m 2(m-j)n_{m-j+1}}r^{2(n-n_m)}, \tag{11}$$

where $K = (n_1, n_2, \cdots, n_m)^T$ is an m-dimensional vector. The total probability of photon-number-resolution is

$$P(\{0,1\}^m, n) = n! \underbrace{\sum_{n_1=0}^{1} \cdots \sum_{n_m=0}^{1}}_{\sum_{j=1}^{m} n_j = n} t^{2(\sum_{j=1}^{m}(m-j)n_{m-j+1})} r^{2(n-n_m)} \tag{12}$$

$$= n! \underbrace{\sum_{n_1=0}^{1} \cdots \sum_{n_m=0}^{1}}_{\sum_{j=1}^{m} n_j = n} T^{\sum_{j=1}^{m}(m-j)n_{m-j+1}} R^{(n-n_m)}. \tag{13}$$

Note that our goal is to split the n input photons over m modes such that each more have either zero or one photon, no matter what modes get the photons. When all beam splitters are identical, the most constrained is the first one as its reflectivity must be much less than $1/n$. However, this approach isn't optimal since the subsequent modes will gradually see fewer photons and can therefore afford larger reflectivities without running the risk of detecting more than one photon. Also, at the end of the device, the last beam splitter should clearly be balanced since the constraint is symmetric for both its output ports. Bearing all this in mind, a symmetrized device appears to be the optimal choice. We investigate it next

SYMMETRIC SEGMENTED DETECTOR

Lossless case

Now we consider the case where the beam splitters have reflectivity $R_j = \frac{1}{m-j+1}$, still in the lossless case ($\eta = 1$). It is easy to see that the probability of getting k APD clicks (where each click may result from one or several simultaneous photons) from m modes, given n input photons, $P_m(k|n)$ is

$$P_m(k|n) = \binom{m}{k} \underbrace{\sum_{n_1=1}^{n} \cdots \sum_{n_m=1}^{n}}_{\sum_{j=1}^{k} n_j = n} \frac{n!}{\prod_{i=1}^{k} n_i!} X, \tag{14}$$

where X is given by

$$X = [(R_1)^{n_1}(T_1)^{n-n_1}][(R_2)^{n_2}(T_2)^{n-n_1-n_2}]\cdots [(R_{m-1})^{n_{m-1}}(T_{m-1})^{n-n_1-n_2\cdots-n_{m-1}}]. \tag{15}$$

Using $R_j = \frac{1}{(m-j+1)}$, and $R_j + T_j = 1$ yields the simplification

$$X = \frac{1}{m^n}. \tag{16}$$

Considering the number of possible configurations, we get

$$P_m(k|n) = \frac{n!}{m^n} \binom{m}{k} \underbrace{\sum_{n_1=1}^{n} \cdots \sum_{n_m=1}^{n}}_{\sum_{j=1}^{k} n_j = n} \frac{1}{\prod_{i=1}^{k} n_i!}. \tag{17}$$

These conditional probabilities are plotted in Fig.4 for

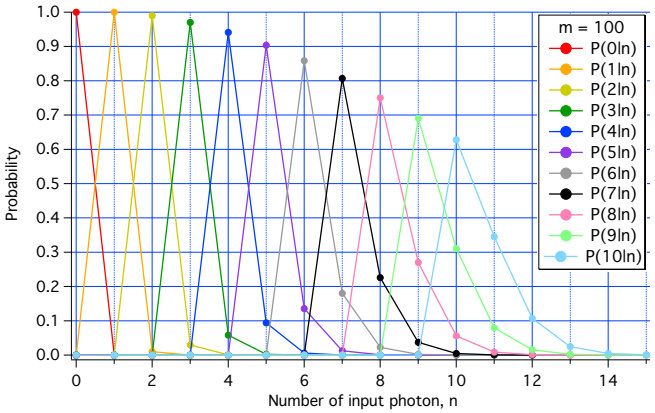

FIG. 4: Conditional probabilities $P_m(k|n)$ versus n, for $m = 100$ APDs and $\eta = 1$.

$m = 100$. Unsurprisingly, they increase for larger photon numbers as m increases (see supplemental material, for m up to 2000). This translates directly into the POVM purities, plotted in Fig.5. As can be seen in that figure,

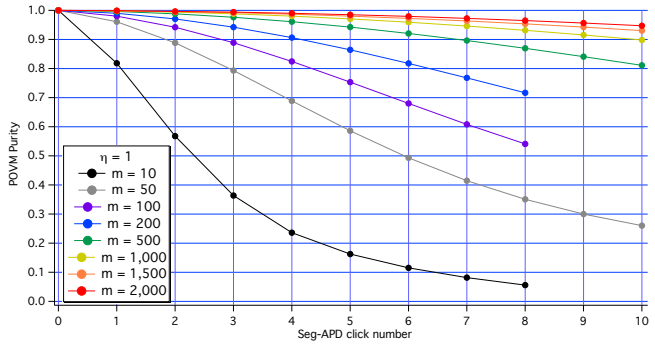

FIG. 5: POVM purity, versus click number k, for different numbers m of APDs.

reasonably good PNR performance can be reached for $n \sim 10$ with $m \sim 1000$.

Lossy case

We now consider the effect of photon losses in each detection mode, i.e., $\eta < 1$. Again, η should not be misconstrued to be the APD quantum efficiency, which

plays no role in photon losses. (An instance of photon loss would be if a photon went undetected and exited the waveguide, losing its chance for further detection.) We assume that the parameter η is independent of the photon number. The probability to get zero clicks in one mode is

$$P_1(0|n,\eta) = (1-\eta)^n. \tag{18}$$

Likewise, the probability to get one click in one mode is [21]

$$P_1(1|n,\eta) = \sum_{k=1}^{n} \binom{n}{k} \eta^k (1-\eta)^{n-k} = 1-(1-\eta)^n. \tag{19}$$

It is important to note that in the sum over k starts with 1 here because we neglected dark counts. Therefore, Eq. (17) can be generalized to

$$P_m(k|n,\eta) = n! \left(\frac{1-\eta}{m}\right)^n \binom{m}{k} \underbrace{\sum_{n_1=0}^{n} \cdots \sum_{n_m=0}^{n}}_{\sum_{j=1}^{k} n_j = n} \left\{ \frac{1}{\prod_{j=1}^{k} n_j!} \prod_{l=n_1}^{n_k} \left[\left(\frac{1}{1-\eta}\right)^l - 1 \right] \right\}. \tag{20}$$

It is worth noting that the probability of getting zero clicks is still the same as the case of one detector, i.e., Eq. 18. For $\eta < 1$ the computer simulations run extremely slowly for higher values of m (reminiscent of the boson sampling problem). We calculated the conditional probabilities at $m = 50$ for $\eta = 0.9, 0.99, 0.999$, and plot the highest losses for illustration in Fig.**??**. Plots for other values of η's are included in the supplementary material. The degradation of the count probability with

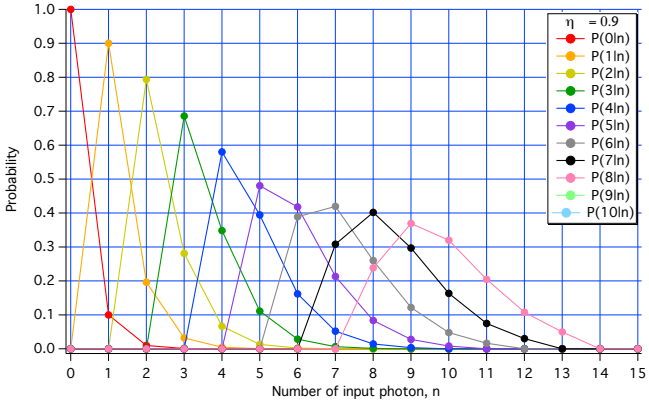

FIG. 6: Conditional probabilities $P_m(k|n)$ versus n, for $m = 50$ APDs and $\eta = 0.9$.

photon loss is evident, compared to Fig.4. Also recall that $\eta = 0.9$ means 10% loss per mode which is a very poor performance. The purity calculation, displayed in

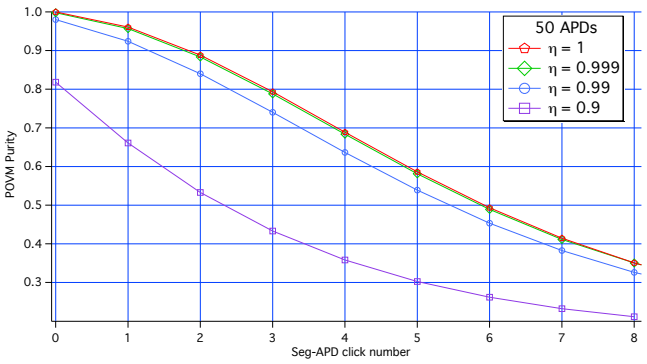

FIG. 7: POVM purity, versus click number k, for several values of η at $m = 50$

Fig.7, is particularly illuminating. Indeed, it is clear that, as η increases beyond the low $eta = 0.9$ level, the photon losses have decreasing to negligible ($\eta = 0.999$) effect on purity, which is essentially limited by m, as per Fig.5. This is an interesting result. It is likely that the same level of photon loss may have a more detrimental effect as m increases, however, the exact scaling of this effect is not yet known, due to the long computation times for the nonideal case.

CONCLUSION

We carried out the theoretical evaluation of the photon-count POVM for the segmented detector. Results show that PNR detection is indeed achievable in the ideal case. This opens a new path to PNR devices that operate at room temperature and can be manufactured with available integrated photonic technology. The number of integrated APDs appears to be, to a large extent, the dominant factor toward high-quality PNR detection. While photon losses must also be taken in to account, of course, it is important to note that they do not include the quantum efficiency of the APDs, by design of the segmented detector. The reduction of photon losses will therefore only involve passive optical design considerations, a notable difference with butt-coupled tree-splitting detectors.

ACKNOWLEDGEMENTS

We are grateful to Joe Campbell, Seth Bank, Aye L. Win, Rafael Alexander, Ben Godek, Sharon S. Philip, Bargav Jayaraman, and Oshin Jakhete for stimulating discussions. This work was supported by the U.S. Defense Advanced Research Projects Agency (DARPA).

[1] E. Knill, R. Laflamme, and G. J. Milburn, Nature **409**, 46 (2001).

[2] J. C. Zwinkels, E. Ikonen, N. P. Fox, G. Ulm, and M. L. Rastello, Metrologia **47**, R15 (2010).

[3] J. L. O'Brien, A. Furusawa, and J. Vuckovic, Nat Photon **3**, 687 (2009).

[4] B. G., G. M., and R. BercheraI., Nat Photon **4**, 227 (2010).

[5] N. Sangouard, C. Simon, J. c. v. Minář, H. Zbinden, H. de Riedmatten, and N. Gisin, Phys. Rev. A **76**, 050301 (2007).

[6] P. Kok, H. Lee, and J. P. Dowling, Phys. Rev. A **65**, 052104 (2002).

[7] M. Ramilli, A. Allevi, V. Chmill, M. Bondani, M. Caccia, and A. Andreoni, J. Opt. Soc. Am. B **27**, 852 (2010).

[8] A. Divochiy, F. Marsili, D. Bitauld, A. Gaggero, R. Leoni, F. Mattioli, A. Korneev, V. Seleznev, N. Kaurova, O. Minaeva, G. Gol'tsman, K. G. Lagoudakis, M. Benkhaoul, F. Levy, and A. Fiore, Nat Photon **2**, 302 (2008).

[9] C. M. Natarajan, L. Zhang, H. Coldenstrodt-Ronge, G. Donati, S. N. Dorenbos, V. Zwiller, I. A. Walmsley, and R. H. Hadfield, Opt. Express **21**, 893 (2013).

[10] F. Mattioli, Z. Zhou, A. Gaggero, R. Gaudio, S. Jahanmirinejad, D. Sahin, F. Marsili, R. Leoni, and A. Fiore, Superconductor Science and Technology **28**, 104001 (2015).

[11] B. E. Kardynał, S. S. Hees, A. J. Shields, C. Nicoll, I. Farrer, and D. A. Ritchie, Applied Physics Letters **90**, 181114 (2007), http://dx.doi.org/10.1063/1.2735281.

[12] A. J. Shields, M. P. O'Sullivan, I. Farrer, D. A. Ritchie, R. A. Hogg, M. L. Leadbeater, C. E. Norman, and M. Pepper, Applied Physics Letters **76**, 3673 (2000), http://dx.doi.org/10.1063/1.126745.

[13] D. Rosenberg, A. E. Lita, A. J. Miller, and S. W. Nam, Phys. Rev. A **71**, 061803 (2005).

[14] A. E. Lita, A. J. Miller, and S. W. Nam, Opt. Express **16**, 3032 (2008).

[15] D. Achilles, C. Silberhorn, C. Śliwa, K. Banaszek, and I. A. Walmsley, Opt. Lett. **28**, 2387 (2003).

[16] M. J. Fitch, B. C. Jacobs, T. B. Pittman, and J. D. Franson, Phys. Rev. A **68**, 043814 (2003).

[17] F. Piacentini, M. P. Levi, A. Avella, M. López, S. Kück, S. V. Polyakov, I. P. Degiovanni, G. Brida, and M. Genovese, Opt. Lett. **40**, 1548 (2015).

[18] A. C. Elitzur and L. Vaidman, Foundations of Physics **23**, 987 (1993).

[19] S. J. van Enk, arXiv:1705.09640 [quant-ph] (2017), arXiv:1705.09640 [quant-ph].

[20] S. J. van Enk, arXiv:1705.09033 [quant-ph] (2017), arXiv:1705.09033 [quant-ph].

[21] M. O. Scully and W. E. Lamb, Jr, Phys. Rev. **179**, 368 (1969).

Appendix 2. Segmented waveguide photodetector with 90% quantum efficiency

Research Article | Vol. 26, No. 10 | 14 May 2018 | OPTICS EXPRESS 12499
Optics EXPRESS

Segmented waveguide photodetector with 90% quantum efficiency

QIANHUAN YU, KEYE SUN, QINGLONG LI, AND ANDREAS BELING*

Department of Electrical and Computer Engineering, University of Virginia, Charlottesville, VA 22904, USA
ab3pj@virginia.edu

Abstract: We demonstrate a novel InGaAsP/InP segmented waveguide photodetector based on directional couplers. By matching the imaginary parts of the propagation constants of the even and odd modes, we designed a photodetector with 6 elements, each with an absorber volume of only 19 μm^3 and a bandwidth of 15 GHz, that has an internal quantum efficiency (QE) of 90% at 1550 nm wavelength corresponding to 1.13 A/W.

OCIS codes: (230.5160) Photodetectors; (230.5170) Photodetectors.

References and links

1. D. Wake, T. P. Spooner, S. D. Perrin, and I. D. Henning, "50 GHz InGaAs edge-coupled PIN photodetector," Electron. Lett. **27**(12), 1073–1075 (1991).
2. Y. Wang, Z. Wang, Q. Yu, X. Xie, T. Posavitz, M. Jacob-Mitos, A. Ramaswamy, E. Norberg, G. Fish, and A. Beling, "High-Power Photodiodes With 65 GHz Bandwidth Heterogeneously Integrated Onto Silicon-on-Insulator Nano-Waveguides," IEEE J. Sel. Top. Quantum Electron. **24**(2), 1–6 (2017).
3. M. N. Draa, J. Bloch, D. Chen, D. C. Scott, N. Chen, S. B. Chen, X. Yu, W. S. Chang, and P. K. L. Yu, "Novel directional coupled waveguide photodiode-concept and preliminary results," Opt. Express **18**(17), 17729–17735 (2010).
4. M. S. Islam, T. Jung, T. Itoh, M. Wu, D. L. Sivco, and Y. Cho, "Velocity-matched distributed photodetectors with pin photodiodes," in *International Topical Meeting on Microwave Photonics MWP 2000*, pp. 217–220 (2000).
5. R. Nehra, C. H. Chang, A. Beling, and O. Pfister, "Photon-number-resolving segmented avalanche-photodiode detectors," arXiv:1708.09015 [physics.ins-det] (2017).
6. F. J. Effenberger and A. M. Joshi, "Ultrafast, dual-depletion region, InGaAs/InP pin detector," J. Lightwave Technol. **14**(8), 1859–1864 (1996).
7. Q. Li, K. Sun, K. Li, Q. Yu, P. Runge, W. Ebert, A. Beling, and J. C. Campbell, "High-Power Evanescently-coupled Waveguide MUTC Photodiode with >105 GHz bandwidth," J. Lightwave Technol. **35**(21), 4752–4757 (2017).
8. A. Yariv, "Coupled-mode theory for guided-wave optics," IEEE J. Quantum Electron. **9**(9), 919–933 (1973).
9. V. R. Chinni, T. C. Huang, P. K. Wai, C. R. Menyuk, and G. J. Simonis, "Crosstalk in a lossy directional coupler switch," J. Lightwave Technol. **13**(7), 1530–1535 (1995).
10. D. Marcuse, "Theory of the Directional Coupler," in *Theory of Dielectric Optical Waveguides* (1991).
11. Z. Li, H. Pan, H. Chen, A. Beling, and J. C. Campbell, "High-saturation-current modified uni-traveling-carrier photodiode with cliff layer," IEEE J. Quantum Electron. **46**(5), 626–632 (2010).

1. Introduction

High speed and high quantum efficiency photodiodes (PDs) are key devices in optical communications, sensing, and microwave photonics. To overcome the well-known bandwidth-efficiency trade-off in normal incidence PDs, side-illuminated or waveguide-photodiodes have been developed [1–3]. Waveguide PDs provide high responsivity and short carrier transit time since electrical and optical transports are not collinear. As most waveguide PDs are butt- or evanescently coupled, their responsivity primarily scales with the length of the absorption layer which can negatively impact the bandwidth and dark current in high-responsivity PDs.

In this paper, we demonstrate a monolithically integrated InP-based p-i-n segmented waveguide photodetector consisting of 6 PDs that are coupled to one waveguide. Optical coupling from the waveguide into the PD absorber and back into the waveguide was accomplished by using a vertical directional coupler design. Light that is not absorbed by the

#324614 https://doi.org/10.1364/OE.26.012499
Journal © 2018 Received 21 Feb 2018; revised 11 Apr 2018; accepted 24 Apr 2018; published 1 May 2018

Optics EXPRESS

first PD couples back into the waveguide and is absorbed in one of the following PDs. We show that the segmented photodetector can achieve near-unity quantum efficiency by using an array of 32 μm long photodiodes with an absorber thickness as small as 30 nm. Compared to the single directional coupled waveguide photodiode in ref [3], our segmented waveguide photodetector achieves higher responsivity and larger bandwidth. We believe that this type of photodetector has potential applications in travelling wave PDs with velocity-matched electrodes [4], and low dark-count photon-number resolving detectors [5] which require minimized absorber volumes and high quantum efficiency.

2. Coupled waveguide design

Figure 1(a) shows the proposed photodiode cross-section. The passive waveguide (WG1) is embedded between two lower index cladding layers and serves as the input waveguide of the photodetector. The upper cladding layer is used to separate WG1 from the second waveguide, the absorption waveguide (WG2). Adding these extra layers does not sacrifice bandwidth performance because they serve as electron drift region similar to the collection layer in dual-depletion region [6] and uni-traveling carrier PDs [7]. The light coupling process in and out of the PD can be recognized as a co-directional coupler problem as illustrated in Fig. 1(b). To ensure complete coupling, the goal is to achieve phase match, i.e. matching the propagations constants of the modes in WG1 and WG2.

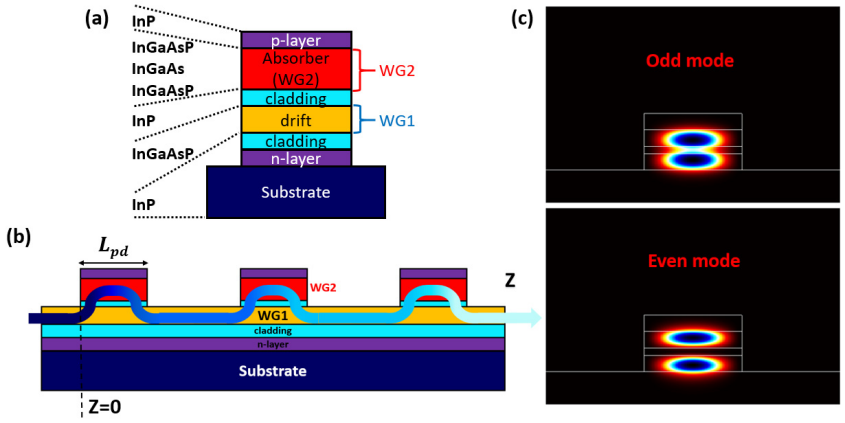

Fig. 1. (a) Cross-section of waveguide photodiode; (b) Light propagating in the segmented waveguide photodetector; (c) Intensity distribution of the anti-symmetric (odd) and symmetric (even) supermodes in the cross-section.

Figure 1(c) shows the intensity distribution of the symmetric (even) and anti-symmetric (odd) supermodes in the cross-section. Based on the theory of mode coupling [8,9], the field distribution $\varnothing_1(z)$ in WG1 and $\varnothing_2(z)$ in WG2 can be represented by adding the even mode field φ_e and the odd mode field φ_o [10]:

$$\begin{aligned}\varnothing_1(z) &= a_1\varphi_e \exp(-i\beta_e z) + a_2\varphi_o \exp(-i\beta_o z)\\ \varnothing_2(z) &= a_3\varphi_e \exp(-i\beta_e z) + a_4\varphi_o \exp(-i\beta_o z)\end{aligned} \quad (1)$$

where β_e and β_o stand for the corresponding propagation constants of these two modes and a_1, a_2, a_3 and a_4 are the coupling coefficients. When light is launched into WG1 at z = 0, it follows:

$$\varnothing_2(0) = a_3\varphi_e + a_4\varphi_o = 0 \quad (2)$$

Optics EXPRESS

In order to ensure low radiation loss, light has to completely couple back from WG2 into WG1 at the rear facet of the PD, hence it is necessary to make $\varnothing_2(l_{pd})=0$. Combining with the initial conditions (Eq. (2), the propagation constant of the odd and even modes should follow:

$$\exp\left[-i(\Delta\beta)l_{pd}\right]=1 \tag{3}$$

here △β is the difference between the even and odd mode propagation constants defined as: $\Delta\beta=\beta_e-\beta_o$. Defining $\Delta\beta_r$ and $\Delta\beta_i$ to be the real and imaginary parts of Δβ, Eq. (3) becomes:

$$\exp\left(\Delta\beta_i l_{pd}\right)\exp\left(-i\Delta\beta_r l_{pd}\right)=1. \tag{4}$$

In order to satisfy above equation, it is imperative to make $\Delta\beta_i=0$. This means, that the propagation constants of the odd and even modes have the same imaginary part. Or, in other words, only when even and odd modes attenuate at the same rate, a complete transfer of optical power between WG1 and WG2 is possible. Moreover, the PD length l_{pd} is concluded to be multiples of the beat length l, defined as:

$$l=2/\Delta\beta_r. \tag{5}$$

3. Simulation

To calculate the field distributions and propagation constants, we used the commercial software Fimmwave. In the design process we started from the simplified structure as shown in Fig. 1(a). Since changing the thickness of the cladding layer between WG1 and WG2 will change β_o and β_e simultaneously, we kept this parameter to be 220 nm to ensure sufficient field overlap between WG1 and WG2. At the same time the thickness of WG1 should be thick enough to ensure minimal field overlap with the highly doped n-contact layer and to prevent free-carrier absorption. However, a thick WG1 layer decreases the coupling efficiency from WG1 to WG2 owing to a better mode confinement. In the design we chose a 500 nm thick WG1 that can provide both, a low free-carrier absorption and a strong coupling. For moderate absorption in the first PD, the thickness of InGaAs in WG2 cannot be too thick. Sandwiching an only 30-nm thin InGaAs layer between the two InGaAsP layers results in a similar propagation constant of WG1 and WG2 with a low effective absorption coefficient in WG2.

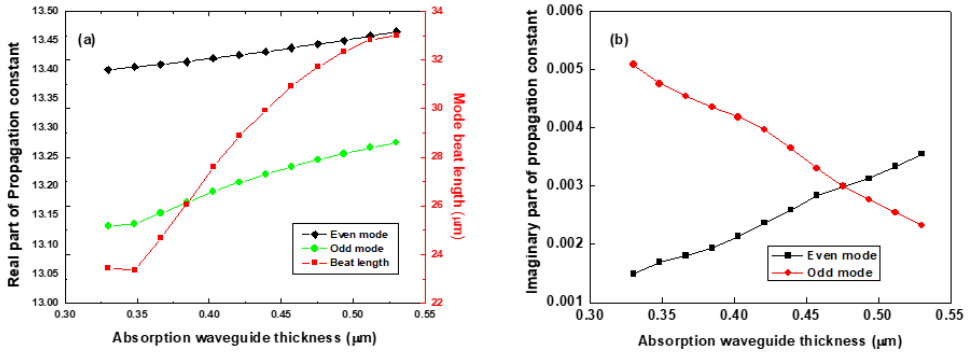

Fig. 2. (a) Real part of propagation constant and mode beat length vs. WG2 thickness. (b) Imaginary part of propagation constants vs. WG2 thickness.

Optics EXPRESS

After adopting two InGaAsP layers sandwiching a 30 nm InGaAs layer as WG2, the relationships between real part of the propagation constants (β_r) and thickness of WG2 are shown in Fig. 2(a). Here, the WG2 thickness is the total thickness of the InGaAs absorption layer and the InGaAsP layers. The β_r of the odd and even mode are both linear with the thickness of WG2. Using Eq. (5), the beat length determined by the difference of the even and odd modes' propagation constants is also shown in Fig. 2(a). The beat lengths range from 23 μm to 33 μm when the thickness of WG2 changes from 0.3 μm to 0.55 μm. In order to ensure that light couples back from WG2 to WG1, the PD length can only be an integral multiple length of the beat length. For the 30 nm thick InGaAs layer being sandwiched by two 220 nm thick InGaAsP layers, each segmented PD element should be around 30 μm. Figure 2(b) shows the simulated imaginary parts of the propagation constants (β_i) of the odd and even modes. We found that β_i of the even mode increases with WG2 thickness while the odd mode behaves vice versa. When the thickness of WG2 is 470 nm, both modes exhibit the same β_i , i.e Eq. (4) is satisfied. According to Fig. 2(a), the beat length is 32 μm in this situation.

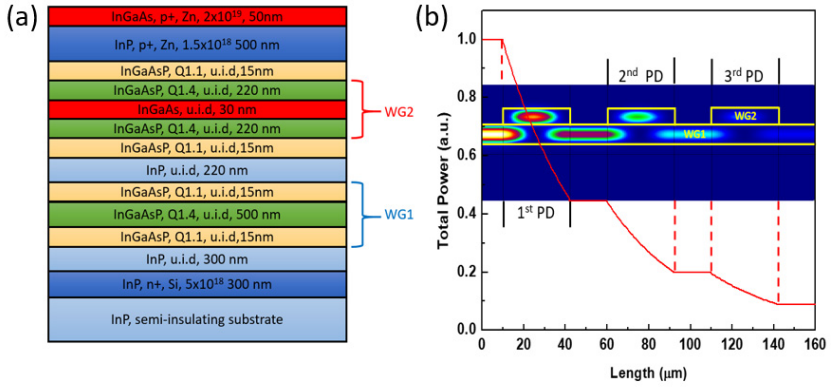

Fig. 3. (a) Epitaxial layer structure for segmented waveguide photodetector. (b) Simulation of the total power in the segmented waveguide photodetector with 3 PDs and a width of 20 μm.

Figure. 3(a) shows the complete epitaxial layer structure of the segmented waveguide photodetector that was grown on InP substrate by metal organic chemical vapor deposition. The 300 nm thick Si-doped InP layer serves as the n-type contact layer followed by an intrinsic 300 nm thick InP layer as the lower cladding. We used a 500 nm thick intrinsic InGaAsP layer as WG1 and a 220 nm thick intrinsic InP cladding layer to separate WG1 and WG2. Two InGaAsP layers sandwich the 30 nm thick InGaAs absorption layer to form WG2. The p-type contact layer is composed of a 500 nm thick highly doped InP and a 50 nm thick top InGaAs layer. We used InGaAsP Q1.1 layers to reduce the band-discontinuities at the heterojunction interfaces between the InP and InGaAsP Q1.4 layers [11]. To ensure that only the fundamental mode propagates in the passive waveguide regions, we designed an 800 μm-long tapered input waveguide. The waveguide width is 4 μm at the input (facet) and matches the PD width at its opposite end. Our simulations revealed that fundamental mode propagation can be maintained throughout the entire segmented waveguide photodetector. Figure 3(b) shows the simulated total power in the 20 μm-wide segmented photodetector with 3 elements. It can be seen that in each PD the light power decays exponentially. Assuming a lossless WG1, the power remains constant in the regions between PD segments. The simulation also predicts that the light couples completely back into WG1 at each PD's rear end.

Optics EXPRESS

4. Fabrication and characterization

A double mesa process was used to fabricate the PDs. To address the tight alignment tolerance between feeding waveguide and photodiode mesa, we used a process that defines both features in one step. The fabrication flow is summarized in Fig. 4. After blanket deposition of the p-metal, we patterned a SiO_2 hard mask and formed a ridge structure. The first mesa etch stopped at the InP n-contact layer to define WG1. Then, the n-metal was deposited. Next, a second hard mask was used to form WG2 and the n-mesa. By this way, we achieved that WG1 and WG2 have a uniform width. AuGe/Ni/Au and Ti/Pt/Au were used for n-metal and p-metal contacts, respectively. Photodiodes were connected to gold-plated pads through air-bridges, as shown in Fig. 5(b). Finally we cleaved the waveguide facet for input light coupling.

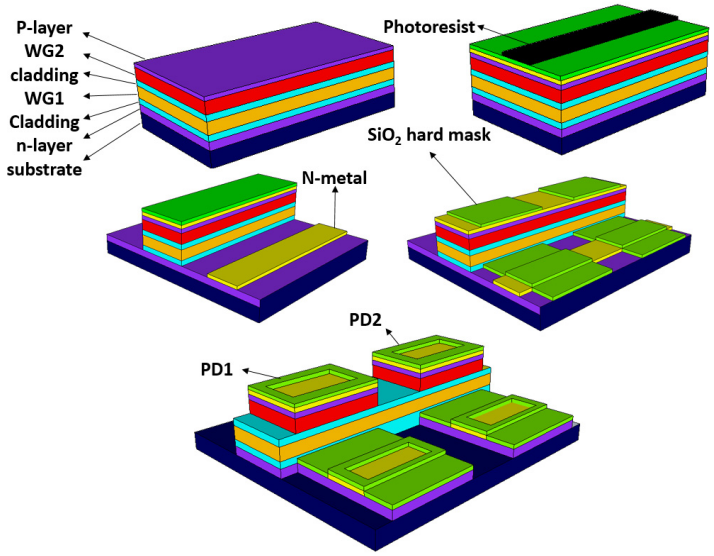

Fig. 4. Fabrication process to achieve uniform width for WG1 and WG2.

To account for uncertainties of the material refractive indices in our simulations we fabricated arrays with photodiode's lengths ranging from 20 μm to 40 μm. All PDs in an array were probed individually. We measured uniform I-V characteristics with dark currents of 1 μA at 3 V reverse voltage. We expect that the dark current can be further reduced with an appropriate side wall passivation.

The frequency responses of single PDs are shown in Fig. 5(c). The data was obtained under large-signal modulation by using an optical heterodyne setup at 1550 nm. It can be seen that a smaller PD area leads to higher bandwidth owing to the reduced capacitance. A photodiode with an active area of 300 μm^2 reached a bandwidth of 20 GHz which is higher than the bandwidth of the directional coupled waveguide photodiode in ref [3]. We estimated the transit time limited bandwidth to be 20 GHz, while the RC-limited bandwidths of the 1200 μm^2 and 300 μm^2 PDs were 34 GHz and 134 GHz, respectively. Hence, the bandwidth of the PD with an area of 300 μm^2 is mainly limited by carrier transit time effects which may explain the difference in roll-off at higher frequencies.

Optics EXPRESS

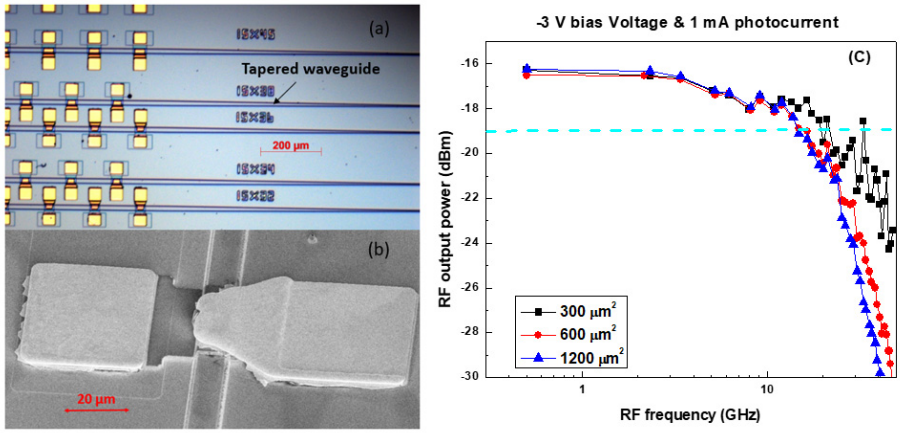

Fig. 5. (a) Microscope picture of fabricated segmented waveguide photodetector, (b) SEM pictures of PD and waveguide, (c) Bandwidth measurements of single photodiodes with different areas from the same wafer.

Using a lensed fiber with 2.5 μm spot size diameter, the quantum efficiency was measured as a function of PD length in single waveguide photodiodes. First we measured several 300 μm long single PDs to characterize the coupling loss from the fiber to the waveguide. According to our simulation, a 300 μm long PD should have an internal QE of 99%. Based on the measured external QE of (35 ± 2) %, the coupling loss from the fiber into the waveguide was calculated to be 4.5 dB. In the analysis, 1.5 dB loss are attributed to reflection at the facet since no anti-reflection coating was used. The remaining loss of 3 dB agrees with the simulated coupling loss due to mode mismatch from the fiber mode to the waveguide mode.

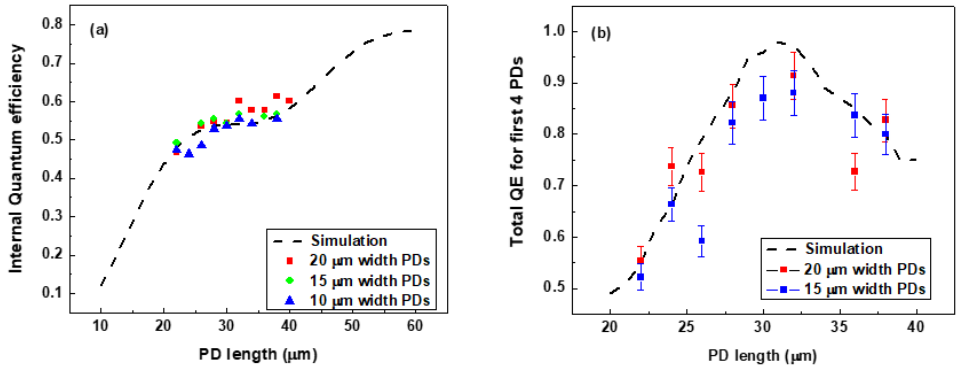

Fig. 6. (a) Measured internal QE of single PDs with different widths vs. PD length. The simulated internal QE (dashed line) showed negligible dependence on PD width. (b) Total internal QE of the segmented waveguide photodetector at a reverse bias of 3 V. The error bars come from the uncertainty in measuring the external QE of several 300 μm-long PDs that were used to determine the fiber coupling loss.

Using 4.5 dB as the coupling loss, Fig. 6(a) shows the internal QE of the first PD in segmented waveguide photodetectors with different PD lengths at a reverse bias of 3 V. The data shows that the QE only depends weakly on PD width. For a fixed width, longer PDs consistently show higher QE owing to the longer absorption length. As expected and due to mode beating phenomena, the QE scales in a non-linear fashion with PD length. This explains the relatively flat region around the calculated beat length of 30 μm in Fig. 6(a), which indicates that in this region the QE does not significantly increase as light couples back into WG1.

Optics EXPRESS

The total QE of 6 element segmented waveguide photodetectors with 15 and 20 μm widths are shown in Fig. 6(b). To determine the internal QE we added the photocurrents of the first 4 PDs in the array that were measured simultaneously, and corrected for the 4.5 dB input coupling loss. As expected from simulation, the contributions from the 5th and the 6th PDs in the array were negligible. The results show that the total internal QE increases for PD lengths larger than are 20 μm. At 32 μm PD length, the QE reaches its peak value around 90% corresponding to 1.13 A/W measured at a photocurrent of 1.7 mA. For longer PDs, the radiation loss prevails leading to a decrease in total QE. The black line in Fig. 6(b) shows the total QE by simulation. It can be seen that the measurement agrees well with the simulation within the error bars. We believe that the scattered nature of the data can be attributed to the fact that different devices came from two different chips with somewhat different facet quality. The fact that the measurement exhibits excess loss can be explained by the following reasons. First, the refractive indices that we used in the simulation may not be accurate. Together with small variations in the epitaxial layer thicknesses this may lead to a mismatch of the propagation constants of WG1 and WG2. Moreover, we did not include any waveguide loss between PD segments in our simulations.

5. Conclusion

A novel segmented waveguide photodetector based on a directional coupler design has been demonstrated. By matching the imaginary parts of the propagation constants of the even and odd modes in the design, a 6 element photodiode array achieves an internal responsivity as high as 1.13 A/W in agreement with simulations. We believe that this design finds applications in travelling wave PDs and in recently proposed photon number resolving detectors that benefit from near-unity quantum efficiency and minimized active volumes.